J. Iron Steel Res. Int. (2018) 25:433–441
https://doi.org/10.1007/s42243-018-0054-y

ORIGINAL PAPER

Effect of Mg addition on formation of intragranular acicular ferrite in heat-affected zone of steel plate after high-heat-input welding

Long-yun Xu[1,2] · Jian Yang[2] · Rui-zhi Wang[3] · Wan-lin Wang[1] · Yu-nan Wang[3]

Received: 5 May 2017 / Revised: 13 June 2017 / Accepted: 23 June 2017 / Published online: 20 April 2018

Abstract
The effects of Mg content, inclusion size, and austenite grain size on the intragranular acicular ferrite (IAF) nucleation in heat-affected zone of steel plate after high-heat-input welding of 400 kJ/cm were investigated by welding simulation and observation using a scanning electron microscope equipped with an energy dispersive spectrometer and an optical microscope. The IAFs are observed in steel with Mg addition, and the volume fraction of IAF is as high as 55.4% in the steel containing 0.0027 mass% Mg. The MgO–Al_2O_3–Ti_2O_3–MnS inclusions with size around 2 μm are effective nucleation sites for IAF, whereas Al_2O_3–MnS inclusions are impotent to nucleate the acicular ferrite. The prior-austenite grain (PAG) size distribution in low Mg steel is similar to that in steel without Mg addition. The austenite grain with size about 200 μm is favorable for the IAF formation. In the steel with high Mg content of 0.0099%, the growth of PAG is greatly inhibited, and PAG sizes are smaller than 100 μm. Therefore, the nucleation of IAF can hardly be observed.

Keywords Heat-affected zone · Inclusion · Intragranular acicular ferrite · Magnesium deoxidation · High-heat-input welding · Steel plate

1 Introduction

It is well known that the most effective method to improve the toughness of heat-affected zone (HAZ) of steel plate after high-heat-input welding is the oxide metallurgy technology [1], which is to make use of oxide inclusions or other kinds of inclusions and precipitates as nucleation sites of intragranular acicular ferrite (IAF) or pinning the growth of austenite grain.

It is widely accepted that the oxysulfides complex inclusions have been termed as effective nucleants for IAF [2]. Many mechanisms of IAF nucleation on inclusions have been proposed, including (1) reduction of interfacial energy [3], (2) decrease in lattice mismatch [4, 5], (3) lessening thermal strains around the inclusions [6, 7], and (4) formation of solute depletion zone around the inclusions [8, 9]. Badu [10] suggested that the increase of chemical driving force resulting from the solute depletion zone is one of the most probable mechanisms of IAF nucleation on inclusions. Besides the chemical composition of inclusion, inclusion size also affects the heterogeneous nucleation of IAF obviously [11].

Nowadays, strong deoxidizer, such as Mg, has been utilized to develop advanced oxide metallurgy technology. As a deoxidization product of Mg, MgO particle was effective in inhibiting the growth of austenite grain in the HAZ of low-carbon steel [12–14]. Zhu et al. [15] found that the toughness of HAZ was improved significantly by adding 0.005 mass% Mg to the Ti-bearing low-carbon steel, since the pinning particles were formed after Mg addition. Besides, the effects of Mg on inclusion modification and microstructural control have also been reported. Chai et al. [16] suggested that a trace amount addition of Mg was able to refine the Ti-based inclusions. Kim et al. [17] have studied the effect of Mg on the variation of inclusions and microstructures during the solidification of steel after the molten steel was deoxidized by Mn–Si–Ti,

✉ Jian Yang
yang_jian@t.shu.edu.cn

1 School of Metallurgy and Environment, Central South University, Changsha 410083, Hunan, China

2 State Key Laboratory of Advanced Special Steel, Shanghai University, Shanghai 200072, China

3 Steelmaking Research Department, Research Institute, Baoshan Iron and Steel Co., Ltd., Shanghai 201999, China

and the results indicated that Mg addition was beneficial for the heterogeneous nucleation of IAF. It is widely accepted that an increased austenite grain size promotes the formation of IAF [18, 19]. Wen and Song [20] reported that the percentage of IAF in steel is greatly increased with the increase of Mg range from 0 to 0.0054%. When the Mg content in steel is relatively high, the pinning effect must be taken into consideration [15]. Therefore, the effect of Mg content on the formation of IAF should be further investigated if the Mg content is changed in a large range.

In the present work, the effect of Mg content on the nucleation of IAF in HAZ of steel plates after high-heat-input welding is investigated with the Mg content changed in a large range. The main purpose of this paper is to clarify the mechanisms of HAZ microstructural control in steel with Mg deoxidation.

2 Experimental procedure

Table 1 shows the chemical compositions of the experimental steel samples. Steel M27 was selected as the sample containing low-level Mg content of 0.0027%, while M99 was selected as the sample containing high-level Mg content that was up to 0.0099%. The Mg content in steel was controlled by addition of different amount of Ni–Mg alloy during deoxidation process. Since Mg is a strong deoxidizing element, the content of Mg dissolved in solid steel is very low, which should be negligible. The Mg generally exists in steel in the form of oxide inclusions. For comparison, a conventional Al-killed steel without Mg addition termed as M0 was used in present study. Each sample was melted in a 50 kg vacuum induction furnace with sintered magnesia lining. About 40 kg of pure iron was first melted, and lime (CaO) was added as top slag to assure considerably low oxygen potential in slag. A proper amount of deoxidants, Mn, Si, Al, Ti, and/or not Mg, were added to obtain the target steel compositions. The initial oxygen contents of the melt before deoxidation in the present experiments were about 0.0050% for Mg deoxidation. Then, the melt was cast into an ingot with the size of 120 mm × 180 mm × 240 mm. Each ingot was then hot rolled by thermo-mechanical control process (TMCP) into a steel plate of the thickness of 50 mm. The detail of TMCP was described in the previous paper [21].

In order to evaluate the HAZ toughness of the experimental steel plates, simulating welding experiments were carried out with a Gleeble 3800 thermal simulation tester (Dynamic system INC., USA). The steel sample for simulating welding experiments was cut down from the position which was 1/4 width and 1/4 length of steel plate from its edge. The peak welding temperature was 1400 °C, with the holding time of 3 s. Then, the sample was cooled from 800 to 500 °C in 385 s, which was designed to simulate the electrogas arc welding with the heat input of 400 kJ/cm for the steel plate of 50 mm in thickness. The Charpy absorbed energy was measured at − 20 °C.

Specimens were then taken from the simulated welding HAZ, and the surfaces in parallel with the fracture cross sections after Charpy impact test were polished and prepared for the characterization of inclusion and microstructure. In order to observe the HAZ microstructure, these polished steel samples were etched by using 4% nital solution. Then, the characteristics of the microstructure in HAZ of the steel samples were investigated through an optical microscope (OM, DM 2500 M, Leica Microsystems, Wetzlar, Germany). The volume fractions of main components in HAZ microstructures, such as grain boundary ferrite (GBF), ferrite side plate (FSP), upper bainite (Bu), IAF, and polygonal ferrite (PF), were quantitatively determined by using the point counting method on a 50-point grid with a minimum of 25 visual fields with 100 times magnification, which were taken at randomly selected locations for each specimen by OM.

In order to investigate the relationship between inclusions and the microstructure formed around the inclusions in HAZ, the microstructure of each sample was observed using a scanning electron microscope (SEM, EVO MA25, Carl Zeiss, Oberkochen, Germany) equipped with energy dispersive spectrometer (EDS, Oxford Instruments, UK) with a 1500 magnification. The total observed areas on the SEM photographs of M0, M27, and M99 were 3.89, 1.05, and 0.94 mm^2, respectively. The details of microstructure and the compositional variation in inclusions were examined with a 5000 magnification by SEM–EDS. Inclusions with the size smaller than 0.2 μm were not counted in this investigation.

Table 1 Chemical compositions of experimental steels (mass%)

Steel	C	Si	Mn	Ti	Mg	Al	O	N	S	Fe
M0	0.078	0.20	1.50	0.0120	–	0.0260	0.0022	0.0014	0.0050	Balance
M27	0.081	0.17	1.45	0.0096	0.0027	0.0010	0.0040	0.0040	0.0060	Balance
M99	0.077	0.20	1.53	0.0110	0.0099	0.0020	0.0024	0.0028	0.0040	Balance

These specimens were re-polished and then etched at 50 °C using a mixed agent (saturated picric acid + detergent + distilled water) to reveal the prior-austenite grain (PAG) boundary. Then, the size of PAG was measured with Image-Pro Plus software by the method of averaging the long axis and short axis in the grain from the OM observed micrographs.

3 Results and discussion

3.1 Effect of Mg content on HAZ microstructures

In the previous study, the evolution of inclusions with the increase of Mg content in steel from 0 to 0.0099% has been investigated [21]. It was found that the typical inclusions comprised central oxides and peripheral MnS. In addition, the central oxides were changed from Al_2O_3 to MgO–Al_2O_3–Ti_2O_3 and MgO with increasing Mg from 0 to 0.0027 and 0.0099%, respectively. It was also found that with increasing Mg addition, the size of inclusions was decreased, and the number density of inclusions was increased. The thermodynamic relationship between Mg and the source of oxidation is shown as follows:

(1) The dissolved Mg in the melt reacts with the dissolved oxygen, which can be written as

$$[\mathrm{Mg}] + [\mathrm{O}] = \mathrm{MgO}_{(\mathrm{inclusion})} \quad (1)$$

(2) In M27, the Mg content in steel is at low level (0.0027%), and the primary Al_2O_3 and Ti_2O_3 inclusions are partly reduced by [Mg], which can be written as

$$3[\mathrm{Mg}] + 4\mathrm{Al_2O_{3(inclusion)}} = 3\mathrm{MgO}\cdot\mathrm{Al_2O_{3(inclusion)}} + 2[\mathrm{Al}] \quad (2)$$

$$3[\mathrm{Mg}] + 4\mathrm{Ti_2O_{3(inclusion)}} = 3\mathrm{MgO}\cdot\mathrm{Ti_2O_{3(inclusion)}} + 2[\mathrm{Ti}] \quad (3)$$

(3) In M99, the Mg content in steel is at high level (0.0099%), and the primary Al_2O_3 and Ti_2O_3 inclusions are completely reduced by Mg, which can be written as

$$3[\mathrm{Mg}] + \mathrm{Al_2O_{3(inclusion)}} = 3\mathrm{MgO_{(inclusion)}} + 2[\mathrm{Al}] \quad (4)$$

$$3[\mathrm{Mg}] + \mathrm{Ti_2O_{3(inclusion)}} = 3\mathrm{MgO_{(inclusion)}} + 2[\mathrm{Ti}] \quad (5)$$

The optical HAZ microstructures of M0, M27, and M99 after simulated high-heat-input welding are illustrated in Fig. 1. The volume fractions of different microstructural components (GBF, Bu, FSP, IAF, and PF) were examined quantitatively using point counting method for 25 fields of each steel at a magnification of 100, as shown in Table 2. The Charpy absorbed energy results at − 20 °C for the steel plate after welding with high heat input of 400 kJ/cm have been reported in previous paper [22]. The average Charpy absorbed energy of M0, M27, and M99 is 27, 179, and 199 J, respectively. The excellent HAZ toughness has been achieved in steel plates with Mg deoxidation.

For steel M0, the HAZ microstructure consisted of a large amount of FSP, as well as parts of Bu and GBF as shown in Fig. 1a–c. With the addition of Mg in steel M27, large quantities of IAF were observed, which were surrounded by GBF, as shown in Fig. 1d–f. The volume fraction of IAF in M27 is as high as 55.40%, as shown in Table 2. It is largely increased by comparison with the results reported by Li et al. [23], in which the volume fraction of IAF was relatively low with about 13% in steel containing 0.0026% Mg. Moreover, in the steel with high-level Mg content up to 0.0099%, the volume fraction of IAF is as low as 3.20%, and that of PF is increased largely up to 95.20%, as shown in Fig. 1g–i and Table 2.

Figure 2 shows the observation results of the microstructures by SEM with magnifications of 1000 and 5000, respectively. As can be seen in Fig. 2a, the parallel FSPs in the steel M0 grew from austenite grain boundary and went through the whole austenite grain. This type of structure was regarded as brittle microstructure, which caused the deterioration of HAZ toughness [19]. The nucleation of ferrite laths on inclusions was not observed in this steel sample. However, the inclusions acting as nucleant of ferrite laths were observed easily in steel M27, as shown in Fig. 2d, which was marked by a black arrow. In the steel M99 with high-level Mg content, ferrites were in evenly distributed polygonal shapes, named as PF, with sizes usually less than 30 μm, as shown in Fig. 2e. Similar microstructure mainly comprising PF was also observed in high Zr steel by Jiang et al. [24]. However, these PF that they found were with sizes larger than 200 μm. It is also found that inclusion with small size was located within the PF grain, as shown in Fig. 2f.

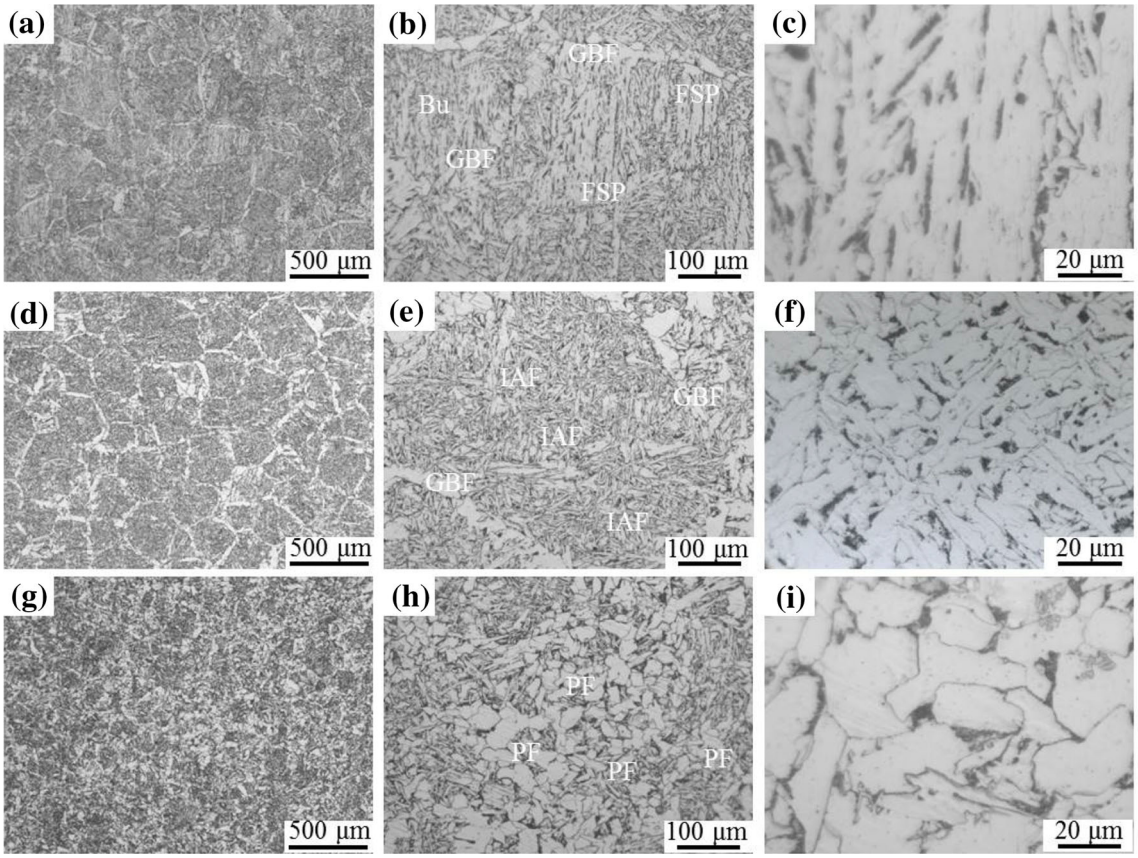

Fig. 1 HAZ microstructures of experimental steels. **a–c** M0; **d–f** M27; **g–i** M99

Table 2 Volume fractions of GBF, FSP, PF, and IAF in steels (vol.%)

Steel	GBF	FSP	Bu	IAF	PF
M0	22.80	49.00	21.60	0.00	6.60
M27	35.00	1.60	2.00	55.40	6.00
M99	0.60	0.40	0.60	3.20	95.20

3.2 Effect of inclusion composition and size on IAF nucleation

In this section, the analysis results of inclusions for the steel samples of M0, M27, and M99 are based on the examination of inclusions in HAZ microstructures using SEM–EDS. The number of inclusions examined in M0, M27, and M99 is 344, 448, and 537 in the observed areas of 3.89, 1.05, and 0.94 mm^2, respectively.

Figure 3 shows SEM micrographs of typical ferrite grains associated with inclusions in steel samples M0, M27, and M99, respectively. As can be seen in Fig. 3a, in steel M0, EDS analysis result indicates that the inclusion located within FSP is composed of Al_2O_3–MnS. This type of inclusions in steel M0 was ineffective for inducing the formation of IAF. It is seen in low Mg steel M27 that the inclusion consisting of MgO–Al_2O_3–Ti_2O_3–MnS can act as nucleant of IAF, as shown in Fig. 3b. In high Mg steel M99, the composition of typical inclusion is MgO–MnS, as shown in Fig. 3c.

The frequency of nucleant was defined as the ratio of the number of inclusions worked as the nucleation sites of IAFs to the number of total inclusions in HAZ. The calculated result is shown in Fig. 4. The frequency of nucleants in steel M27 is as high as 9.30%, and those in M0 and M99 are both near zero.

Figure 5 shows the size distribution of all inclusions and the inclusions as nucleants for IAF in steel M27. It is found that the size of most inclusions is between 0.8 and 1.8 μm and most of IAF nucleants is range from 1.6 to 2.8 μm. It is also found in Fig. 5 that there are only small parts of inclusions acting as IAF nucleants even in steel M27. The probability of inclusions for nucleating acicular ferrite lath at a given size range is defined as the ratio of the number of inclusions worked as the nucleant of IAF to the number of total inclusions at the same given size range [11, 25]. Figure 6 documents the calculated results as a function of inclusion size. It is found that an increased inclusion size markedly enhances the probability of an IAF nucleation in

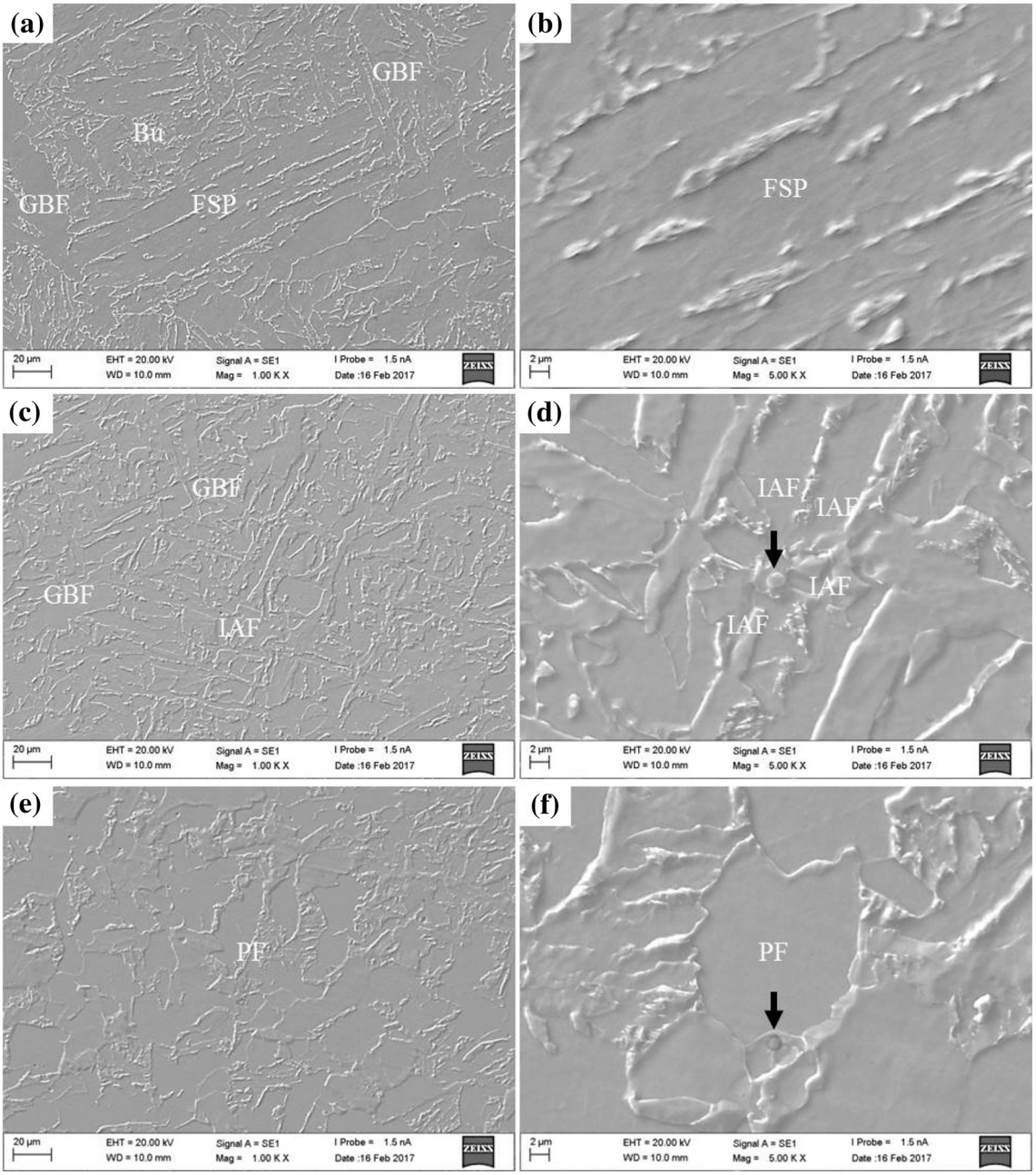

Fig. 2 SEM micrographs of HAZ microstructures in experimental steels. **a**, **b** M0; **c**, **d** M27; **e**, **f** M99

M27. However, M0 and M99 show totally different tendency. The probability of IAF nucleation in both of them is almost zero, which is independent of the inclusion sizes.

In previous studies, Lee et al. [11] and Mu et al. [25] reported the nucleation probability of oxide inclusions of different sizes. The tendency of their results seems to be similar as present results found in steel M27. However, their results of the minimum sizes of nucleant inclusions are apparently smaller than the present result of 1.00 μm, which are 0.30 and 0.85 μm, respectively. In the study of Lee et al. [11], such inclusions were located in the low-carbon steel weld. And the result reported by Mu et al. [25] was based on the investigation of the inclusions in as-cast steel with Ti_2O_3 powder addition. Obviously, the thermal histories in the steel weld and as-cast steel are different with that in HAZ. It is notable that the role of inclusions on the microstructures in steel weld, as-cast steel and HAZ might be different, which should be investigated further. It is also found in Fig. 3b that the widths of IAF laths are around 2 μm, which have almost the same size as those of nucleant inclusions.

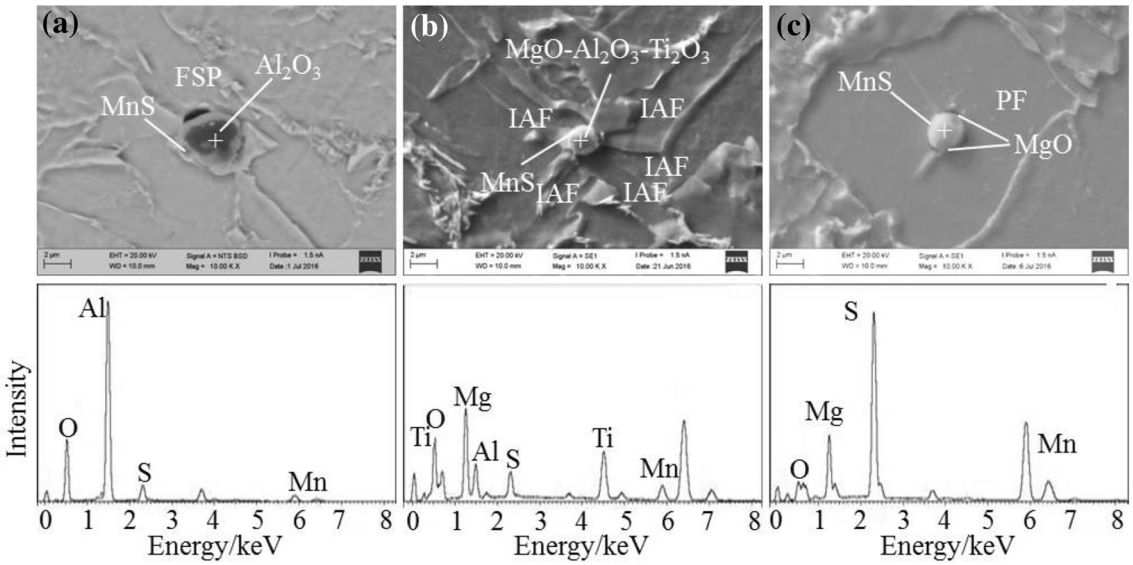

Fig. 3 SEM micrographs and EDS analysis results of typical ferrite grains associated with inclusions in steels. **a** M0; **b** M27; **c** M99

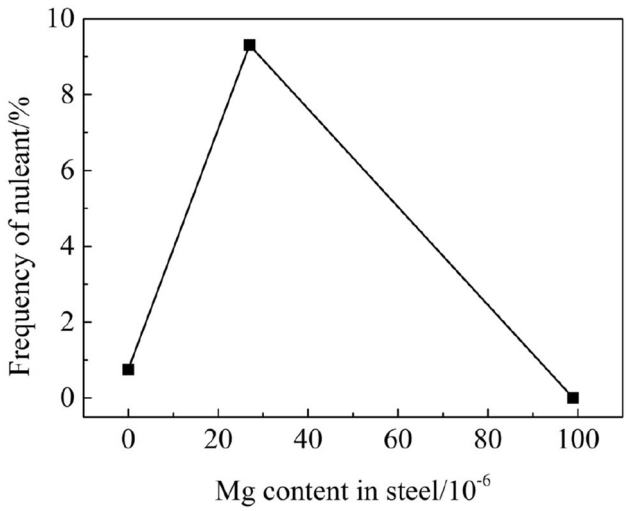

Fig. 4 Change in frequency of nucleant for IAF with Mg content in steel

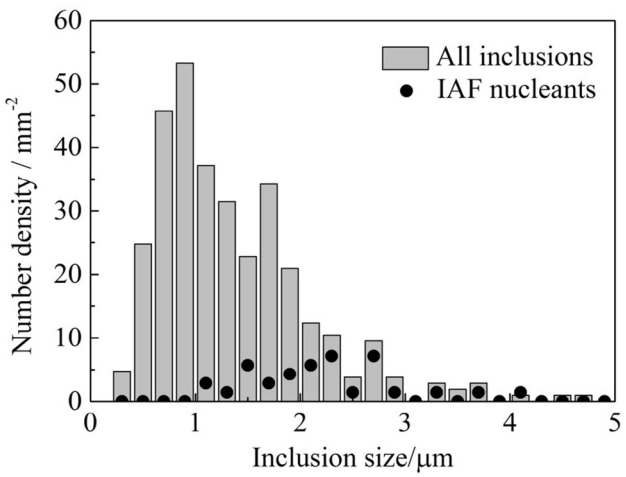

Fig. 5 Size distribution of all inclusions and inclusions as nucleants for IAF in M27

3.3 Effect of austenite grain size on IAF formation

Figure 7 shows the typical optical micrographs of the PAGs in HAZs of steel M0, M27, and M99. It can be seen clearly in Fig. 7a, b that the GBFs are located along the austenite grain boundaries, which are signed by black arrows. The size distributions of PAGs in steel M0, M27, and M99 are shown in Fig. 8. The number of PAGs measured in each steel sample was more than 300. It is seen that the PAGs size distribution of steel M0 shown in Fig. 8a is similar to that of steel M27 shown in Fig. 8b. The mean PAG size in steel M0 is 220 μm, which is a little larger than that in M27, 206 μm. In steel M99, most of PAGs have the sizes around 60 μm, being even as small as 30 μm, as shown in Fig. 8c.

In the conventional Al-killed steel M0 and low Mg steel M27, austenite grains grow significantly because HAZs were held for a considerable time period at a high temperature of around 1400 °C. It is reported that the volume fraction of IAF was increased with increasing austenite grain size from 100 to 400 μm [18]. In steel M0, the austenite grain sizes were appropriate to the formation of IAF. But the main inclusions in steel M0 are Al_2O_3–MnS inclusions, which were ineffective nucleant for IAF, as shown in Fig. 3a. As a result, IAF was hardly observed inside the austenite grains in steel M0 instead of FSP and Bu, as shown in Figs. 1b and 2a. By contrast, in steel M27, there existed well-developed IAF structures inside the

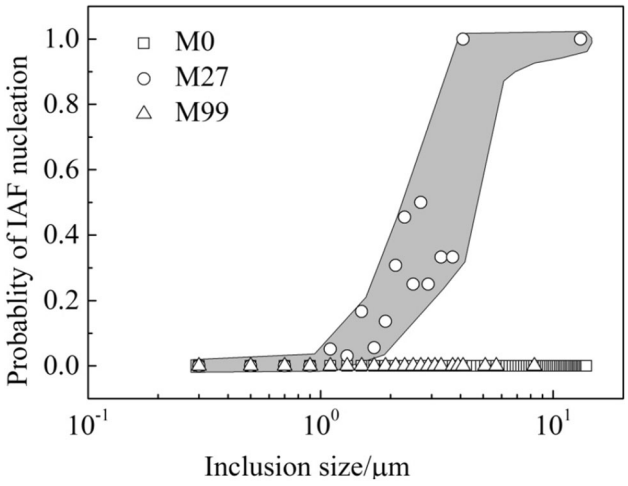

Fig. 6 Relationship between nucleation potency of IAF and inclusion size at different Mg contents

austenite grains with the similar sizes. In steel M99, the growth of austenite grain during welding process was intensely prohibited so that the sizes of PAGs were decreased sharply to less than 100 μm, as shown in Fig. 8c. Generally, when the austenite grain size is larger than 100 μm, it can contribute to IAF nucleation [18, 26, 27]. Otherwise, the $\gamma \rightarrow \alpha$ transformation will firstly take place at the boundary triple points to form PFs [22]. Thus, the volume fraction of PFs in steel M99 is as high as 95.20%, as shown in Table 2. Meanwhile, the IAF in steel M99 is hardly observed.

3.4 Mechanism of IAF formation from inclusions

It is seen in Fig. 3b that the nucleant inclusion in steel M27 mainly consists of Mg, Al, Ti, Mn, O, and S elements from the EDS analysis result. From the element mapping results

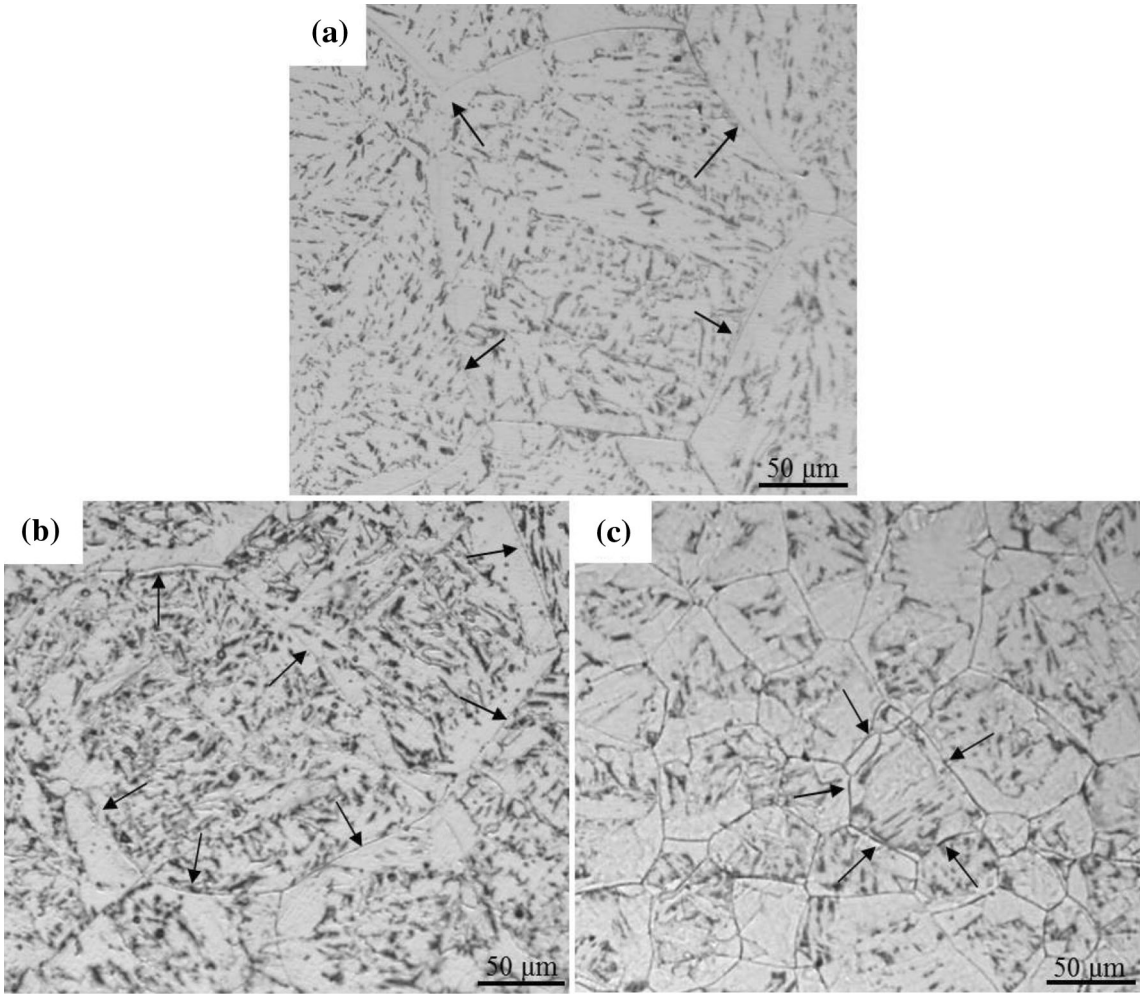

Fig. 7 Optical micrographs of prior-austenite grains in HAZ. **a** M0; **b** M27; **c** M99

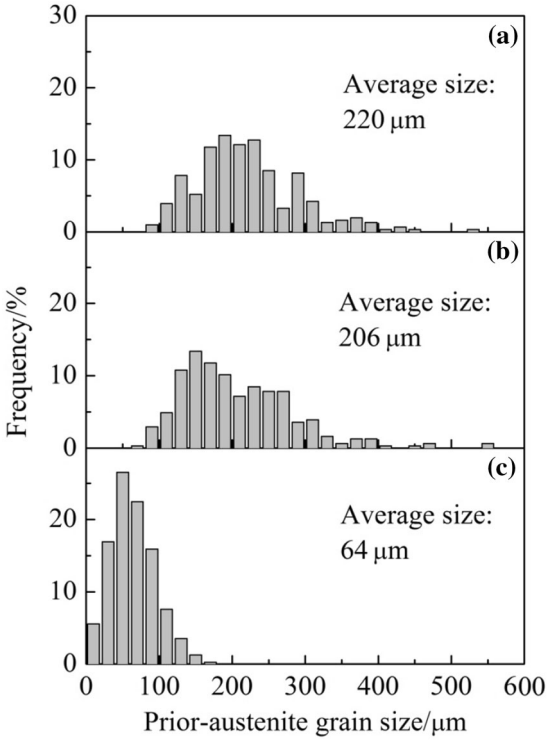

Fig. 8 Size distribution of prior-austenite grains in HAZ. **a** M0; **b** M27; **c** M99

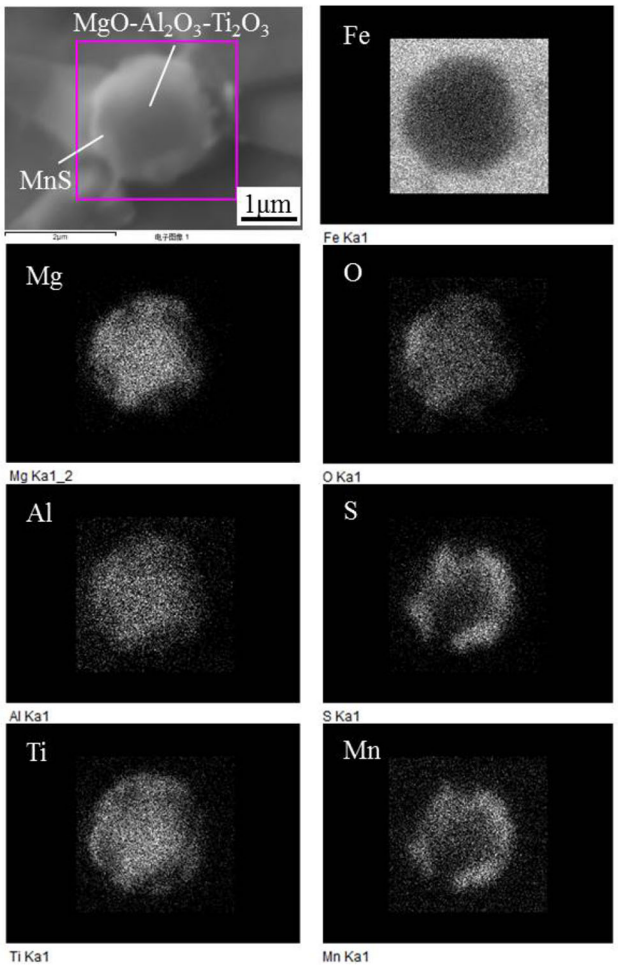

Fig. 9 Elemental mapping pattern of $MgO–Al_2O_3–Ti_2O_3$–MnS inclusion nucleating IAF in M27

shown in Fig. 9, it is seen that the Mg, Al, and Ti in the core part of the inclusion are overlapped with O. It indicates that the central oxide inclusion is homogeneous $MgO–Al_2O_3–Ti_2O_3$ complex inclusion. It is also seen that the MnS phase is covering the central $MgO–Al_2O_3–Ti_2O_3$ inclusion. This type inclusion is usually considered as an effective nucleant for IAF [2, 27, 28]. An Mn-depleted zone (MDZ) can be formed by the MnS precipitation on oxide inclusion during cooling process. Shigesato et al. [29] have reported the direct measurement results of MDZ formed around MnS precipitate. Thus, the MDZ mechanism could be the dominating factor of IAF nucleation on the inclusion in steel M27.

It is well known that Ti_2O_3 is the most effective nucleant for IAF [30–32]. This is because Ti_2O_3 is with cation vacancies, which contribute to preferential nucleation of MnS precipitate on Ti_2O_3 [33]. In steel M27, Ti_2O_3 in the $MgO–Al_2O_3–Ti_2O_3$ complex inclusion is evenly distributed and directly covered by MnS phase, as shown in Fig. 9. Li et al. [23] have reported that the volume fraction of IAF was relatively low with 13% in the steel containing $MgO–Al_2O_3$–MnS inclusions. Comparing with steel M27, the Mg and Ti contents in the study of Li et al. were at the similar levels except that the Al content was much higher. Thus, there was no Ti_2O_3 in the complex inclusions instead of $MgO–Al_2O_3$–MnS inclusions. It is reasonable to infer that the $MgO–Al_2O_3–Ti_2O_3$–MnS inclusion could act as an effective nucleant for IAF by the formation of MDZ. In addition, the main role of a trace amount addition of Mg was to refine the Ti_2O_3 inclusions by modifying them into Mg-containing complex inclusions in molten steel [16].

The typical Al_2O_3–MnS inclusion in steel M0 has the similar morphology with $MgO–Al_2O_3–Ti_2O_3$–MnS inclusion in steel M27, as shown in Fig. 3. The central part Al_2O_3 was covered by MnS precipitate. This type inclusion is impotent to induce the nucleation of IAF, as shown in Fig. 3a. Al_2O_3 is an anion vacancy oxide [34], and thus it is not in favor of the formation of MDZ. In steel M99, the typical inclusion contains MnS dotted with MgO particles, as shown in Fig. 3c. Due to the PAG in steel M99 is too small, as shown in Fig. 8c, the austenite grain boundaries tend to act as the preferential nucleation sites of ferrites during $\gamma \rightarrow \alpha$ transformation [22]. The ability of inducing the IAF nucleation for MgO–MnS inclusions is greatly retarded.

Figure 10 shows the relation among PAG size, number density of nucleant inclusions, volume fraction of IAF and Mg content in steel. When the Mg content in steel M27 is

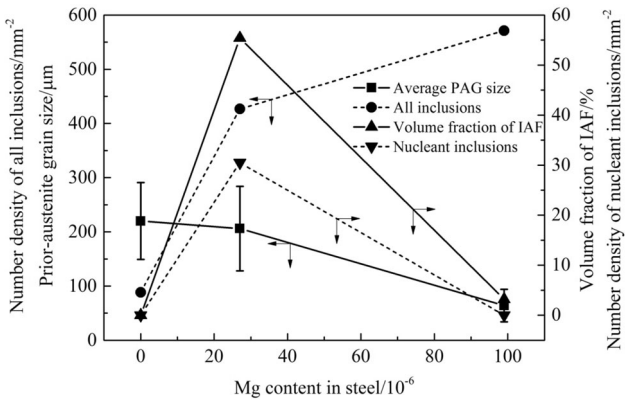

Fig. 10 Relation among prior-austenite grain size, number density of all inclusions, number density of nucleant inclusions, volume fraction of IAF, and Mg content in steel

relatively low with 0.0027%, the sizes of austenite grains are similar with those of steel M0 without Mg addition. Because considerable nucleant inclusions, MgO–Al_2O_3–Ti_2O_3–MnS inclusions, were formed in steel M27, the microstructures inside the austenite grains were changed from Bu and FSP in steel M0 to IAF in steel M27. With increasing Mg content up to 0.0099% in steel M99, the growth of austenite grains during welding process was intensely prohibited by strong pinning effect [14]. As a result, the IAF cannot be formed inside the austenite grain instead of PF growing from austenite grain boundary.

4 Conclusions

1. With Mg content in steel increasing from 0 to 0.0027 and then to 0.0099 mass%, the main heat-affected zone microstructure is changed from ferrite side plate (FSP) and grain boundary ferrite to intragranular acicular ferrite and grain boundary ferrite and then to polygonal ferrite. The average prior-austenite grain size is decreased from 220 to 206 μm and then to 64 μm.
2. Al_2O_3–MnS complex inclusion is impotent to nucleate an acicular ferrite. The inclusions inducing IAF nucleation is complex inclusions consisting of MgO–Al_2O_3–Ti_2O_3 core and MnS shell. Mn-depleted zone should be considered as the main mechanism of IAF formation nucleated by this type complex inclusion.
3. When the Mg content in steel is relatively low with 0.0027%, the formation of IAF is promoted due to the relatively large size of austenite grains and the large number of MgO–Al_2O_3–Ti_2O_3–MnS inclusions with size around 2 μm acting as nucleants. When the Mg content in steel is as high as 0.0099%, the growth of austenite grains is greatly retarded and the sizes of most austenite grains are smaller than 100 μm. As a result, the formation of IAF is inhibited completely instead of PF.

Acknowledgements This research was funded by the National Key Research and Development Program of China (2016YFB0300602).

References

[1] S. Ogibayashi, Nippon Steel Tech. Rep. 61 (1994) 70–76.
[2] J.L. Lee, Y.T. Pan, Metall. Trans. A 24 (1993) 1399–1408.
[3] R.A. Ricks, P.R. Howell, G.S. Barritte, J. Mater. Sci. 17 (1982) 732–740.
[4] J.M. Gregg, H.K.D.H. Bhadeshia, Metall. Mater. Trans. A 25 (1994) 1603–1611.
[5] M. Enomoto, Met. Mater. 4 (1998) 115–123.
[6] T. Yamada, H. Terasaki, Y.I. Komizo, ISIJ Int. 49 (2009) 1059–1062.
[7] H. Nako, Y. Okazaki, J.G. Speer, ISIJ Int. 55 (2015) 250–256.
[8] J.H. Shim, Y.W. Cho, S.H. Chung, J.D. Shim, D.N. Lee, Acta Mater. 47 (1999) 2751–2760.
[9] Y.B. Kang, H.G. Lee, ISIJ Int. 50 (2010) 501–508.
[10] S.S. Babu, Curr. Opin. Solid State Mater. Sci. 8 (2004) 267–278.
[11] T.K. Lee, H.J. Kim, B.Y. Kang, S.K. Hwang, ISIJ Int. 40 (2000) 1260–1268.
[12] A. Kojima, A. Kiyose, R. Uemori, M. Minagawa, M. Hoshino, T. Nakashima, K. Ishida, H. Yasui, Nippon Steel Tech. Rep. 90 (2004) 2–6.
[13] K. Sakata, H. Suito, Metall. Mater. Trans. A 31 (2000) 1213–1223.
[14] K. Zhu, Z.G. Yang, Metall. Mater. Trans. A 42 (2011) 2207–2213.
[15] K. Zhu, J. Yang, R.Z. Wang, Z.G. Yang, J. Iron Steel Res. Int. 18 (2011) No. 9, 60–64.
[16] F. Chai, C.F. Yang, H. Su, Y.Q. Zhang, Z. Xu, J. Iron Steel Res. Int. 16 (2009) No. 1, 69–74.
[17] H.S. Kim, C.H. Chang, H.G. Lee, Scripta Mater. 53 (2005) 1253–1258.
[18] D. Zhang, H. Terasaki, Y.I. Komizo, Acta Mater. 58 (2010) 1369–1378.
[19] D.S. Sarma, A.V. Karasev, P.G. Jönsson, ISIJ Int. 49 (2009) 1063–1074.
[20] B. Wen, B. Song, J. Manuf. Sci. Prod. 13 (2013) 61–72.
[21] J. Yang, L.Y. Xu, K. Zhu, R.Z. Wang, L.J. Zhou, W.L. Wang, Steel Res. Int. 86 (2015) 619–625.
[22] L.Y. Xu, J. Yang, R.Z. Wang, Y.N. Wang, W.L. Wang, Metall. Mater. Trans. A 47 (2016) 3354–3364.
[23] X.B. Li, Y. Min, Z. Yu, C.J. Liu, M.F. Jiang, J. Iron Steel Res Int. 23 (2016) 415–421.
[24] M. Jiang, Z.Y. Hu, X.H. Wang, J.J. Pak, ISIJ Int. 53 (2013) 1386–1391.
[25] W.Z. Mu, P.G. Jönsson, K. Nakajima, ISIJ Int. 54 (2014) 2907–2916.
[26] J.L. Lee, Acta Metall. Mater. 42 (1994) 3291–3298.
[27] M.M. Song, B. Song, C.L. Hu, W.B. Xin, G.Y. Song, ISIJ Int. 55 (2015) 1468–1473.
[28] Z.H. Wu, Z. Wan, G.Q. Li, M. Hiroyuki, T. Fumitaka, Metall. Mater. Trans. B 46 (2015) 1226–1241.
[29] G. Shigesato, M. Sugiyama, S. Aihara, R. Uemori, Y. Tomita, Tetsu-to-Hagane 87 (2001) 93–100.
[30] H. Mabuchi, R. Uemori, M. Fujioka, ISIJ Int. 36 (1996) 1406–1412.
[31] J.L. Lee, Y.T. Pan, ISIJ Int. 35 (1995) 1027–1033.
[32] Z. Zhang, R.A. Farrar, Mater. Sci. Technol. 12 (1996) 237–260.
[33] K. Yamamoto, T. Hasegaw, J.I. Takamura, ISIJ Int. 36 (1996) 80–86.
[34] Z.T. Ma, Control of nonmetallic inclusions in continuously cast steels in view of macro-cleanliness, castability, precipitation modification and grain refinement, Technische Universität Bergakademie Freiberg, Freiberg, 2000.